$RE_5Co_4Si_{14}$ (RE = Ho, Er, Tm, Yb): Silicides Grown from Ga Flux Showing Exceptional Resistance to Chemical and Thermal Attack

James R. Salvador, Christos Malliakas, Jeff R. Gour, and Mercouri G. Kanatzidis*

Department of Chemistry and Center for Fundamental Materials Research, Michigan State University, East Lansing, Michigan 48842

Received November 22, 2004. Revised Manuscript Received January 19, 2005

The compounds $RE_5Co_4Si_{14}$ (RE = Ho, Er, Tm, and Yb) have been synthesized from a Ga flux and characterized by X-ray diffraction. They can also be made by direct combination of the elements with arc melt alloying. All crystallize in the $Lu_5Co_4Si_{14}$ structure type in the monoclinic space group $P2_1/c$ with lattice parameters: $a = 12.3765(15)$ Å, $b = 7.8142(9)$ Å, $c = 7.7330(9)$ Å, $\beta = 98.867(2)°$; $a = 12.337(2)$ Å, $b = 7.7990(14)$ Å, $c = 7.7144(15)$ Å, $\beta = 98.85(3)°$; $a = 12.3140(16)$ Å, $b = 7.778(1)$ Å, $c = 7.705(1)$ Å, $\beta = 98.815(2)°$; and $a = 12.255(3)$ Å, $b = 7.7537(16)$ Å, $c = 7.6730(15)$ Å, $\beta = 98.95(3)°$ for $Ho_5Co_4Si_{14}$, $Er_5Co_4Si_{14}$, $Tm_5Co_4Si_{14}$, and $Yb_5Co_4Si_{14}$, respectively. The compounds are composed of a dense Si/Co framework that is assembled from $[Co_4Si_{10}]$ slabs and $[Si_4]$ zigzag chains. Crystals of the title compounds proved to be remarkably resistant to thermal oxidative attack (up to 1000 °C) as well as chemical attack from concentrated mineral acids and bases. The origin of this behavior can be traced to the details of the crystal structure and the Si-rich nature of the crystal framework.

Introduction

Silicides comprise a technologically important class of compounds with widespread use in semiconductor applications, refractory coatings and in thermal processing applications such as heating elements.[1,2] The source of the refractory character in silicides is the formation of a protective SiO_2 layer[3] that can be stable at elevated temperatures since crystalline SiO_2 does not melt until 1750 °C,[4] although often the oxide layers break down at considerably lower temperatures.[3] One of the leading silicides for refractory applications is $MoSi_2$, which is used extensively in heating elements for high-temperature furnaces. It suffers from several major drawbacks, as do many intermetallic compounds, which limits its applications. Specifically, its extreme brittleness especially at room temperature,[3] its tendency for pesting in low-temperature low-moisture regimes,[5] and its susceptibility to attack by Na_2SO_4, and $NaCO_3$ in melts and hot burner gases.[6] Other binary silicides of transition metals such as Fe_3Si, Ni_3Si,[7] and $TMSi_x$ (TM = transition metal and $x = 2-3$)[8] have also been investigated for refractory applications, and have been found to suffer from brittleness, the same as $MoSi_2$. Si-rich compounds are of interest for a variety of applications where extreme environments would be prevalent because they will likely be less dense than the Ni super alloys, which are currently used in the bulk of aerospace propulsion components. Despite these considerations exploratory research in new complex silicides has been relatively limited.[9−11]

* To whom correspondences should be addressed. E-mail: kanatzid@cem.msu.edu.

(1) (a) Szytula, A.; Leciejewicz, J. *CRC Handbook of Crystal Structures and Magnetic Properties of Rare Earth Intermetallics*; CRC Press: Baton Rouge, 1994; p 110. (b) Anderson, B.; Lundström, T.; Rundqvist, S. *Borides, Silicides, Phosphides*; Methuen & Co. Ltd.: London, 1965.

(2) (a) Fitzer, E. Schlichting, *High-Temperature Corrosion*, Proceedings from a National Association of Corrosion Engineers symposium; Rapp, R. A., Ed.; National Association of Corrosion Engineers: 1983; p 604. (b) Kircher, T. A.; Courtright, E. L. *Mater. Sci. Eng. A* **1992**, *155*, 67. (c) Mueller, A.; Wang, G.; Rapp, R. A.; Courtright, E. L. *J. Electrochem. Soc.* **1992**, *139*, 1266. (d) Petrovic, J. J. *MRS Bull.* **1993**, *18* (7), 35.

(3) Brady, M. P.; Pint, B. A.; Tortorelli, P. F.; Wright, I. G.; Hanrahan, R. J., Jr. *Mater. Sci. Technol.* **2000**, *19* (pt. 2 Corrosion and Environmental Degradation Vol. 2), 229.

(4) *Binary Alloy Phase Diagrams*, 2nd ed.; Massalski, T. B., Ed.; ASM International: New York, 1990; Vol. 2, p 1856.

(5) McKamey, C. G.; Tortorelli, P. F.; Devan, J. H.; Carmichael, C. A. *J. Mater. Res.* **1992**, *7*, 2747.

(6) (a) Schlichting, J. *High Temp.-High Pressures* **1978**, *10*, 241. (b) Schlichting, J. *Spec. Ceram.* **1975**, *6*, 161.

(7) Oliver, J. *High Temperature Ordered Intermetallic Alloys V*; Liu, C. T., Izumi, O., Eds.; Material Research Society: Pittsburgh, 1989; p 833.

(8) Shah, D. M.; Berczik, D.; Anton, D. L.; Hetch, R. *Mater. Sci. Eng. A* **1992**, *155*, 45.

(9) (a) Schoolaert, S.; Jung, W. *Z. Anorg. Allg. Chem.* **2002**, *628*, 1806. (b) Debus, S.; Harbrecht, B. *Z. Anorg. Allg. Chem.* **2001**, *627*, 431. (c) Perrier, C.; Kirschen, M.; Vincent, H.; et al. *J. Solid State Chem.* **1997**, *133*, 473. (d) Perrier, C.; Kreisel, J.; Vincent, H. *J. Alloys Compd.* **1997**, *262*, 71. (e) Salamakha, P. S.; Stepen-Damm, J.; Prots, Y.; et al. *J. Alloys Compd.* **1996**, *242* (1−2), L3−L4. (f) Kotur, B. Y.; Bodak, O. I.; Zavodnik, V. E.; *Kristallografiya* **1985**, *30*, 899.

(10) (a) Prots, Y. M.; Stepien'-Damm, J.; Salamakha, P. S.; Oleksyn, O. Ya.; Sologub, O. L.; Bodak, O. I. *J. Alloys Compd.* **1996**, *240*, 16. (b) Morozkin, A. V.; Seropegin, Y. D.; Bodak, O. I. *J. Alloys Compd.* **1996**, *234*, 143. (c) Stepien'-Damm, J.; Prots, Y.; Salamakha, P. S.; Bodak, O. I.; Morozkin, Y.; Seropegin, Y. D. *J. Alloys Compd.* **1998**, *268*, 177. (d) Tursina, A. I.; Gribanov, A. V.; Seropegin, Y. D.; Bodak, O. I. *J. Alloys Compd.* **2004**, *367*, 142. (e) Tursina, A. I.; Gribanov, A. V.; Seropegin, Y. D.; Bodak, O. I. *J. Alloys Compd.* **2001**, *319*, 145.

(11) (a) Stepien'-Damm, J.; Prots, Y.; Salamakha, P. S.; Bodak, O. I.; Morozkin, Y.; Seropegin Y. D. *J. Alloys Compd.* **1998**, *268*, 177. (b) Salamakha, P.; Sologub, O.; Bocelli, G.; Righi, L. *J. Alloys Compd.* **2000**, *299* (1−2), L6. (c) Rizzoli, C.; Salamakha, P. S.; Sologub, O. L.; Belletti, D.; Goncalves, A. P.; Almeida, M. *J. Alloys Compd.* **2004**, *363*, 217. (d) Salamakha, R.; Rizzoli, C.; Sologub, O. L.; Belletti, D.; Protsyk, O. S.; Goncalves, A. P.; Almeida, A. *J. Alloys Compd.* **2004**, *368*, 269. (e) Ijjaali, I.; Venturini, G.; Malaman, B. *J. Alloys Compd.* **1999**, *282*, 153. (f) Proserpio, D. M.; Chacon, G.; Zheng, C. *Chem. Mater.* **1998**, *10*, 1286.

10.1021/cm047959w CCC: $30.25
Published on Web 03/11/2005

We have been interested in new Si-containing compounds of the type RE/TM/Si (RE = rare earth metal, TM = first- or second-row transition metal) in hopes of discovering new silicides with interesting physical properties[12] including resistance to thermal oxidation. We have used Ga flux with a great deal of success to synthesize a large class of complex silicides and germanides of the type RE/TM/Si,[13] RE/TM/Ga/Si,[14] and RE/TM/Ga/Ge[15] and borosilicides such as $Tb_{1.8}Si_8C_2(B_{12})_3$[16] and β-SiB_3.[17] We have found from this research that quaternary Ga silicides do not form readily as Ga is not easily incorporated into the compounds despite its great molar excess. In these cases Ga plays the role of a nonreactive solvent and is therefore an excellent medium from which to explore complex silicides. This approach can greatly facilitate structural and physiochemical characterization by producing large high-quality crystals.

We present here a series of rare earth cobalt silicides, $RE_5Co_4Si_{14}$ (RE = Ho, Er, Tm, and Yb), synthesized from a Ga flux which crystallize in the $Lu_5Co_4Si_{14}$ structure type.[18] These compounds have been presented previously, along with their Fe analogues, but due to the mis-assignment of the Bravais lattice as orthorhombic instead of the correct primitive monoclinic one, the structure was incorrectly determined and as a result the stoichiometry was erroneously determined to be $RE_3Co_2Si_7$.[19] $RE_5Co_4Si_{14}$ can also be obtained by direct combination of the elements with arc melting, though we could not produce them as pure phases. They have excellent corrosion resistance at temperatures exceeding 900 °C. The crystal structure, chemical inertness, corrosion resistance, and magnetic properties of $RE_5Co_4Si_{14}$ are described.

Experimental Section

Reagents and Synthesis. All reagents were used as-received without further purification and were stored and handled under a N_2 atmosphere in a glovebox. An amount of 1 mmol of the corresponding rare earth metal, Ho metal (−40 mesh powder, 99.9%, Cerac, Milwaukee, WI), Er metal (powder ground from metal chunk, 99.9%, Chinese Rare Earth Information Center, Inner Mongolia, China), Tm metal (powder ground from metal chunk, 99.9%, Chinese Rare Earth Information Center, Inner Mongolia, China), Yb metal (powder ground from metal chunk, 99.9%, Chinese Rare Earth Information Center, Inner Mongolia, China), 1 mmol of Co (−325 mesh, 99.9%, Cerac, Milwaukee, WI), 3 mmol of Si (−325 mesh amorphous powder, 99.999%, Cerac, Milwaukee, WI), and 10 mmol of Ga(3−5 mm pieces, 99.999%, Plasmaterials, Livermore CA) were combined in an Al_2O_3 (alumina) crucible. The crucible and reactants were flame-sealed in a fused silica tube under a reduced atmosphere of 10^{-4} mbar. The reaction was carried out by first heating to 850 °C over the course of 8 h and holding at 850 °C for 72 h before cooling to room temperature over 48 h. The product was isolated by gently warming the product and decanting the excess liquid Ga. Because Ga tends to wet the surface of the products, isolation was completed by soaking the products in a 5 M I_2 dimethyl formamide (DMF) solution (to form soluble GaI_3). Yields were generally >80% based on the rare earth with purities that greatly depended on the rare earth metal used.

$RE_5Co_4Si_{14}$ can also form through a direct combination of the elements with arc melting by combining and cold-pressing the elements in their stoichiometric ratios on the millimole scale also under a N_2 atmosphere in a glovebox. Reactions were run under a gettered Ar atmosphere on a water-cooled copper plate. Reaction melts were flipped and remelted three times in order to ensure a homogeneous distribution of reactants. Yields were nearly quantitative, though pure samples could not be obtained from this method. Purity was not significantly improved by a week of annealing at 950 °C.

Elemental Analysis. Semiquatitative microprobe elemental analysis was performed with a JEOL JSM-35C scanning electron microscope (SEM) equipped with the Noran energy-dispersive spectrometer (EDS). Data were acquired using an accelerating voltage of 20 kV and an acquisition time of 100 s. Several crystals from each reaction were analyzed, and the resulting approximate atomic ratios of 1.2:1:2.2 RE:Co:Si were found. A $SmNiSi_3$ single crystal[13] was used as a standard reference, and after a correction factor was applied the ratios were approximately 1.3:1:3.6 RE:Co:Si. These results agree well with the atomic ratios that were derived from the crystallographic refinement of the structure.

X-ray Crystallography. Single-crystal X-ray diffraction data were collected at room temperature using a Bruker AXS SMART CCD diffractometer with graphite monochromatized Mo Kα (λ = 0.71073 Å) radiation. Unit cell refinement and data merging were done with the SAINT program, and an empirical absorption correction was applied using the program SADABS.[20] The cell of the Tm analogue was originally indexed by SMART as a = 7.705 Å, b = 7.778 Å, and c = 12.314 Å in a monoclinic C Bravais lattice. Inspection of the remaining systematic absences gave the possible space groups *C*2, *Cm*, and *C*2/*m*. *C*2/*m* was the only centrosymmetric space group and was therefore chosen.[21] A satisfactory solution could not be obtained with this space group or any *C*-centered space group and led to a structure containing mixed and partially occupied sites with high residual electron density and atomic ratios that were at odds with elemental analysis. The reason for the mistaken assignment of *C*-centering was due to the $h + k = 2n$ reflections being systematically weak but not absent. As a result of using the primitive lattice, the space group $P2_1/c$ was found to be the correct one. The structure solution obtained in this space group gave a model that was ordered with each site fully occupied and reasonable residual electron density. Further, the atomic ratios obtained from this solution agreed well with those obtained by elemental analysis. The single-crystal data collection

(12) (a) Sieve, B.; Chen, X.-Z.; Henning, R.; Brazis, P.; Kannewurf, C. R.; Cowen, J. A.; Schultz, A. J.; Kanatzidis, M. G. *J. Am. Chem. Soc.* **2001**, *123*, 7040. (b) Sieve, B.; Sportouch, S.; Chen, X.-Z.; Cowen, J. A.; Brazis, P.; Kannewurf, C. R.; Papaefthymiou, V.; Kanatzidis, M. G. *Chem. Mater.* **2001**, *13*, 273. (c) Chen, X.-Z.; Small, P.; Sportouch, S.; Zhuravleva, M.; Brazis, P.; Kannewurf, C. R.; Kanatzidis, M. G. *Chem. Mater.* **2000**, *12*, 252. (d) Zhuravleva, M. A.; Kanatzidis, M. G. *Z. Naturforsch. B−A* **2003**, *58*, 649.
(13) Chen, X.-Z.; Larson, P.; Sportouch, S.; Brazis, P.; Mahanti, S. D.; Kannewurf, C. R.; Kanatzidis, M. G. *Chem. Mater.* **1999**, *11*, 75.
(14) Zhuravleva, M. A.; Chen, X.-Z.; Wang, X. P.; Schultz, A. J.; Ireland, J.; Kannewurf, C. K.; Kanatzidis, M. G. *Chem. Mater.* **2002**, *14*, 3066.
(15) (a) Zhuravleva, M. A.; Wang, X. P.; Schultz. A. J.; Bakas, T.; Kanatzidis, M. G. *Inorg. Chem.* **2002**, *41*, 6056. (b) Zhuravleva, M. A.; Pcioneck, R. J.; Wang, X. P.; Schultz, A. J.; Kanatzidis, M. G. *Inorg. Chem.* **2003**, *42*, 6412.
(16) Salvador, J. R.; Bilc, D.; Mahanti, S. D.; Kanatzidis, M. G. *Angew. Chem., Intl. Ed.* **2002**, *38*, 844.
(17) Salvador, J. R.; Bilc, D.; Mahanti, S. D.; Kanatzidis, M. G. *Angew. Chem., Intl. Ed.* **2003**, *42*, 1929.
(18) Chabot, B.; Parthé, E. *Acta Crystallogr. C* **1986**, *42*, 945.
(19) Yarovets, V. I. Thesis, Ivan Franko University, Lvov, Ukraine, 1978.
(20) (a) *SAINT*, Version 4; Siemens Analytical X-ray Instruments, Inc.: Madison, WI, 1997. (b) Sheldrick, G. M. *SADABS*; University of Göttingen: Göttingen, 1997.
(21) *International Table for Crystallography Vol. 1 Space-Group Symmetry*, 4th ed.; Hahn, T. D., Ed.; Reidel Publishing Co.: Boston, 1983; pp 39−48.

Table 1. Crystallographic Data and Refinement Details for $LnNiGe_2$ (Ln = Dy, Er, Yb, and Lu)[a]

empirical formula	$Ho_5Co_4Si_{14}$	$Er_5Co_4Si_{14}$	$Tm_5Co_4Si_{14}$	$Yb_5Co_4Si_{14}$
formula weight	1453.44	1465.28	1473.60	1494.18
crystal system/	monoclinic/	monoclinic/	monoclinic/	monoclinic/
space group	$P2_1/c$	$P2_1/c$	$P2_1/c$	$P2_1/c$
unit cell dimensions (Å)	$a = 12.376(2)$	$a = 12.337(2)$	$a = 12.3140(16)$	$a = 12.255(2)$
	$\alpha = 90°$	$\alpha = 90°$	$\alpha = 90°$	$\alpha = 90°$
	$b = 7.8142(9)$	$b = 7.799(1)$	$b = 7.778(1)$	$b = 7.7537(16)$
	$\beta = 98.867°$	$\beta = 98.85(3)°$	$\beta = 98.815(2)°$	$\beta = 98.95(3)°$
	$c = 7.7330(9)$	$c = 7.7144(15)$	$c = 7.7053(10)$	$c = 7.6730(15)$
	$\gamma = 90°$	$\gamma = 90°$	$\gamma = 90°$	$\gamma = 90°$
volume/Z	738.94(15)/2	733.3(2)/2	729.28(16)/2	720.2(3)/2
density(calculated) (g/cm^3)	6.533	6.476	6.711	6.890
absorption coefficient (mm^{-1})	31.905	32.974	35.619	37.732
θ range for data collection (deg)	5,2° to 32.14°	1.67 to 27.85°	1.67° to 27.06°	3.12° to 33.78°
index ranges	$-18 \le h \le 18$,	$-15 \le h \le 15$,	$-15 \le h \le 15$,	$-19 \le h \le 15$,
	$-11 \le k \le 11$,	$0 \le k \le 10$,	$-9 \le k \le 9$,	$-11 \le k \le 11$,
	$-9 \le l \le 9$	$0 \le l \le 9$	$-9 \le l \le 3$	$-11 \le l \le 11$
reflections collected/unique/[R(int)	10500/2436/0.0810	4402/1674/0.0424	4826/1565/0.0375	9486/2705/0.0438
data/restraints/parameters	2436/0/108	1674/0/108	156/0/107	2705/0/108
goodness-of-fit on F^2	1.12	0.95	1.142	1.97
final R indices [$I > 2\sigma(I)$] (R1/wR2)	0.0369/0.0662	0.0493/0.1307	0.0427/0.1275	0.0347/0.0714
R indices (all data) (R1/wR2)	0.1105/0.0875	0.0750/0.1465	0.0474/0.1302	0.0460/0.0728
extinction coefficient	0.032(3)	0.079(3)	0.033(3)	0.045(3)
largest diff. peak and hole (e/Å^3)	2.29 and −2.15	5.70 and −3.72	3.514 and −3.497	3.22 and −3.74

[a] $R1 = \Sigma||F_o| - |F_c||/\Sigma|F_o|$ and $wR2 = [\Sigma(|F_o^2 - F_c^2|)^2/\Sigma(wF_o^2)^2]^{1/2}$.

parameters and refinement details for all compounds are given in Table 1. The atomic coordinates and isotropic displacement parameters for each analogue are listed in Table 2.

Crystal twinning was a major difficulty in elucidating the structures of these compounds. Initially, acceptable crystallographic solutions could only be obtained for the Tm and Ho analogues. Data sets on several crystals of $Er_5Co_4Si_{14}$ and $Yb_5Co_4Si_{14}$ were collected but could not be refined, as large residual electron densities remained despite using the solution of the Tm analogue as a starting solution.

Single-crystal X-ray diffraction data of $Yb_5Co_4Si_{14}$ were re-collected at room temperature using a STOE IPDS II diffractometer with graphite monochromatized Mo Kα radiation. Careful inspection of the reciprocal lattice revealed a second twin domain rotated 180° along the *a*-axis. The orientation matrixes of both domains were used for the data reduction by using the X-Area software package. The twinned structure was refined with the JANA2000[22] software by applying the twin law

$$\begin{bmatrix} a' \\ b' \\ c' \end{bmatrix} = \begin{bmatrix} a \\ b \\ c \end{bmatrix} \cdot \begin{bmatrix} 1 & 0 & 0 \\ 0 & -1 & 0 \\ 1/2 & 0 & -1 \end{bmatrix}$$

This led to a successful refinement with very small residuals in the electron density map and reasonable R1 and wR2 values with a refined twin fraction of 45.2(2)%. Because of this success we decided to re-examine old data of $Er_5Co_4Si_{14}$. The data were reduced using the SAINT 6.45 program,[23] which includes a twin support feature. Both domains were taken into account and an empirical absorption correction was applied using the program TWINABS,[24] and JANA2000 software was used for the refinement and a refined twin fraction of 27.5(3)%.

Phase purity was evaluated by powder X-ray diffraction carried out on a Rigaku rotating Cu anode powder diffractometer with Bragg/Brentano geometry. The diffractometer has postdiffraction monochromatization of the Cu Kα line, which was required to cut out the fluorescence of Co. All $RE_5Co_4Si_{14}$ (RE = Ho, Er, Tm, and Yb) phases were identified by comparing the experimental powder pattern to a powder pattern calculated from the single-crystal structure solution.

Other Physical Methods. Differential thermal analysis (DTA) was performed on a Shimadzu DTA-50 differential thermal analyzer with an α-Al_2O_3 standard reference. The samples were heated to 1000 °C at a rate of 10 °C/min and then cooled to 150 °C at the same rate. The cycle was then repeated to determine if the compound melted congruently. Thermal gravimetric analysis (TGA) was performed on a Shimadzu TGA-50 thermal gravimetric analyzer. The sample was heated to 1000 °C at a rate of 10 °C/min under flowing air, held at 1000 °C for 5 min, and then cooled back to room temperature at the same rate.

Magnetic susceptibility measurements were made on selected crystals that were ground and screened by powder X-ray diffraction for phase purity. The samples were cleaned prior to measurement by submersion in concentrated HCl for 20 min to remove Co-containing impurities. Susceptibility measurements were performed with a Quantum Design MPMS SQUID magnetometer in both field-cooled and zero-field-cooled modes at temperatures between 2 and 300 K. All magnetization data were also collected at 5 K with fields sweeping from 55 to −55 kOe.

Results and Discussion

Flux Reaction vs Direct Combination. In the previous report of this structure only the Lu compound was presented,[18] which was produced by arc melt alloying of the elements in their stoichiometric ratios. In this work we repeated the arc-melting synthesis with other rare earth metals (Ho, Er, Tm, and Yb) and found that the "as cast" pellets did produce the target phase as the major component, but a large amount of an unidentified impurity was also present. Annealing did not eliminate these impurities. Several attempts with different temperatures (950 °C and 850 °C) and soaking times (1 and 2 weeks) were attempted without greatly improving the purity of the sample. In fact, the longer annealing step at 950 °C introduced more reflections into the powder patterns that could not be indexed to $RE_5Co_4Si_{14}$ or the original impurity, and the title compounds no

(22) Petricek, V.; Dusek, M. *Jana2000. The Crystallographic Computing System*; Institute of Physics: Praha, 2000.
(23) *SAINT*, version 6.45; Siemens Analytical X-ray Instruments Inc.: Madison, WI, 1997.
(24) Sheldrick, G. M. *SHELXL*; University of Göttingen: Göttingen, 2002.

Table 2. Atomic Coordinates ($\times 10^4$) and Equivalent Isotropic Displacement Parameters ($Å^2 \times 10^3$) for $RE_5Co_4Si_{14}$ (RE = Ho, Er, Tm, and Yb)

atom	Wyckoff position	*x*	*y*	*z*	*U*(eq)[a]
Ho(1)	2b	5000	0	0	4(1)
Ho(2)	4e	8643(1)	2518(1)	−1578(1)	4(1)
Ho(3)	4e	1355(1)	2490(1)	1605(1)	4(1)
Co(1)	4e	4996(2)	3741(3)	1276(3)	8(1)
Co(2)	4e	7491(1)	−4(3)	608(2)	4(1)
Si(1)	4e	5000(4)	−3362(5)	1620(6)	7(1)
Si(2)	4e	6771(5)	−2746(6)	1388(6)	4(1)
Si(3)	4e	6783(3)	61(8)	−2328(4)	4(1)
Si(4)	4e	6777(5)	2751(6)	500(6)	5(1)
Si(5)	4e	6789(3)	−50(8)	3198(4)	5(1)
Si(6)	4e	9413(3)	4988(8)	1124(4)	6(1)
Si(7)	4e	9400(2)	4(8)	1096(4)	4(1)
Er(1)	2b	5000	0	0	4(1)
Er(2)	4e	8647(1)	2519(1)	−1576(2)	3(1)
Er(3)	4e	1350(1)	2490(1)	1602(2)	3(1)
Co(1)	4e	5000(1)	3735(1)	1294(1)	4(1)
Co(2)	4e	7494(2)	0(1)	613(1)	3(1)
Si(1)	4e	4991(1)	−3356(1)	1635(1)	6(1)
Si(2)	4e	6774(1)	−2763(1)	382(1)	7(1)
Si(3)	4e	6786(1)	58(1)	−2306(1)	5(1)
Si(4)	4e	6774(1)	2760(1)	488(1)	3(1)
Si(5)	4e	6791(1)	−50(1)	3204(1)	3(1)
Si(6)	4e	9407(1)	4995(1)	1112(1)	3(1)
Si(7)	4e	9404(1)	1(1)	1084(1)	4(1)
Tm(1)	2b	5000	0	0	7(1)
Tm(2)	4e	8650(1)	2518(1)	−1576(1)	8(1)
Tm(3)	4e	1348(1)	2489(1)	1602(1)	8(1)
Co(1)	4e	4998(1)	3741(2)	1272(2)	7(1)
Co(2)	4e	7501(1)	−2(1)	611(2)	8(1)
Si(1)	4e	4994(2)	−3338(3)	1661(4)	9(1)
Si(2)	4e	6788(3)	−2741(4)	389(5)	10(1)
Si(3)	4e	6784(3)	54(3)	−2314(5)	7(1)
Si(4)	4e	6786(3)	2738(4)	500(5)	7(1)
Si(5)	4e	6789(3)	−55(3)	3187(5)	7(1)
Si(6)	4e	9401(3)	4999(3)	1106(5)	10(1)
Si(7)	4e	9406(3)	8(3)	1092(5)	9(1)
Yb(1)	2b	5000	0	0	5(1)
Yb(2)	4e	8652(1)	2521(1)	−1588(1)	5(1)
Yb(3)	4e	1345(1)	2488(1)	1610(1)	5(1)
Co(1)	4e	4998(1)	3739(1)	1268(1)	6(1)
Co(2)	4e	7502(1)	−1(3)	611(1)	4(1)
Si(1)	4e	4996(3)	−3346(3)	1661(3)	7(1)
Si(2)	4e	6791(5)	−2742(7)	406(6)	5(1)
Si(3)	4e	3201(1)	53(8)	−2315(3)	5(1)
Si(4)	4e	6783(3)	2741(7)	507(6)	6(1)
Si(5)	4e	6789(3)	−62(9)	3191(3)	5(1)
Si(6)	4e	9396(1)	5008(11)	1105(7)	6(1)
Si(7)	4e	9410(1)	−3(11)	1093(7)	6(1)

[a] *U*(eq) is defined as one-third of the trace of the orthogonalized $\mathbf{U}^{ij}$ tensor.

longer appeared to be the majority phase. Presumably, a reaction occurred between $RE_5Co_4Si_{14}$ and the impurity phase, yielding a third, as yet, unidentified phase.

Impure samples prohibit the accurate characterization of these phases and so an alternative synthetic route employing Ga flux was devised. The flux reactions were optimized for time and temperature to yield the largest fraction of $RE_5Co_4Si_{14}$. This was a balance between letting reactions run to completion while trying to minimize the presence of quaternary Ga-containing phases that tended to form over time. The yields of these reactions are typically 80−90%. The fully isolated product consisted of 2 main phases: the target phase and the Co analogue of the hexagonal $RE_{0.67}Ni_2Ga_{5+n-x}Si_x$, which has been reported previously.[25] The exact ratio of the two products depended on the rare earth metal used, but the target phase was generally 60 to 80% of the product. We observed that longer reaction times or higher temperatures favored the quaternary hexagonal phase for every rare earth used. The Ho and Er systems favored the formation of the hexagonal $RE_{0.67}Co_2Ga_{5-x}Si_x$ phase compared to the Tm and Yb. We suspect that this may be due to a size effect. The crystal habits of $RE_5Co_4Si_{14}$ and $RE_{0.67}Co_2Ga_{5+n-x}Si_x$ are sufficiently different to easily separate them mechanically and thereby obtain pure samples for physical characterization. Admittedly, yields of the title compound can be relatively low (50%), especially for the larger rare earth metals such as Ho; however, the advantage of this method of synthesis is the ability to obtain a pure sample of $RE_5Co_4Si_{14}$. The compounds $RE_5Co_4Si_{14}$ grow as stacks of staggered plates. A typical crystal of $Tm_5Co_4Si_{14}$ is shown in Figure 1. It is this stacking that resulted in heavy twinning, which complicated the single-crystal structural analysis of the Er and Yb analogues.

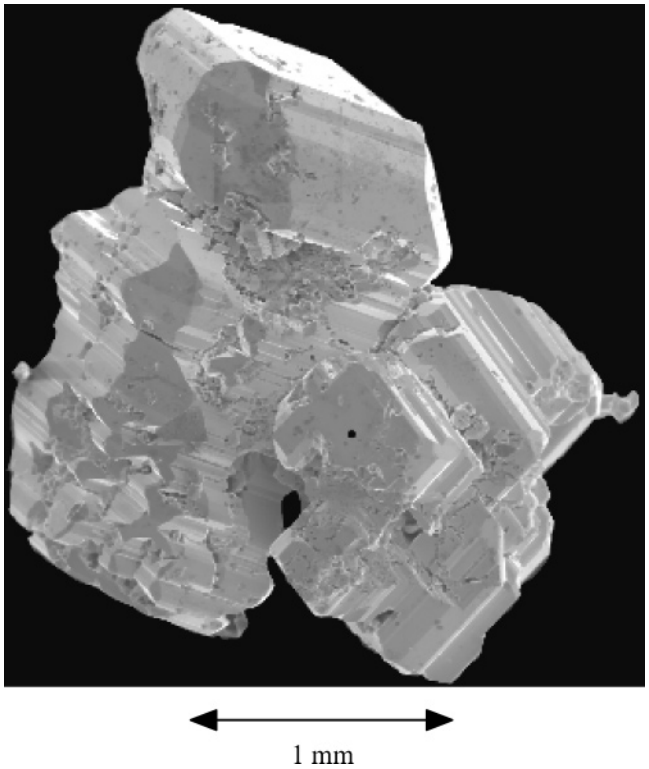

Figure 1. Scanning electron micrograph of $Tm_5Co_4Si_{14}$ crystal cluster. This figure shows the crystal habit and plate stack twinning typical of these samples.

Structure. Because of the isostructural nature of these compounds, we will only describe the structure of the $Tm_5Co_4Si_{14}$ analogue. The title compounds are composed of a dense Si/Co framework that is quite complex when viewed in its entirety, but it can be dissected into several simpler units such as $[Co_4Si_{10}]$ slabs and $^1/_\infty[Si_4]$ zigzag chains. Within the slabs there is a clearly defined Co_2Si_{10} cage, Figure 2A. This cage is made up of two face-sharing square antiprisms. It has a center of symmetry with one crystallographically distinct Co atom (Co(1)) and 5 different Si atoms (Si(1), Si(2), Si(3), Si(4), and Si(5)). The Co(1)−Si distances

(25) Zhuravleva, M. A.; Chen, X.-Z.; Wang, X.; Schultz A. J.; Ireland, J.; Kannewurf, C. K.; Kanatzidis, M. G. *Chem. Mater.* **2002**, *14*, 3066.

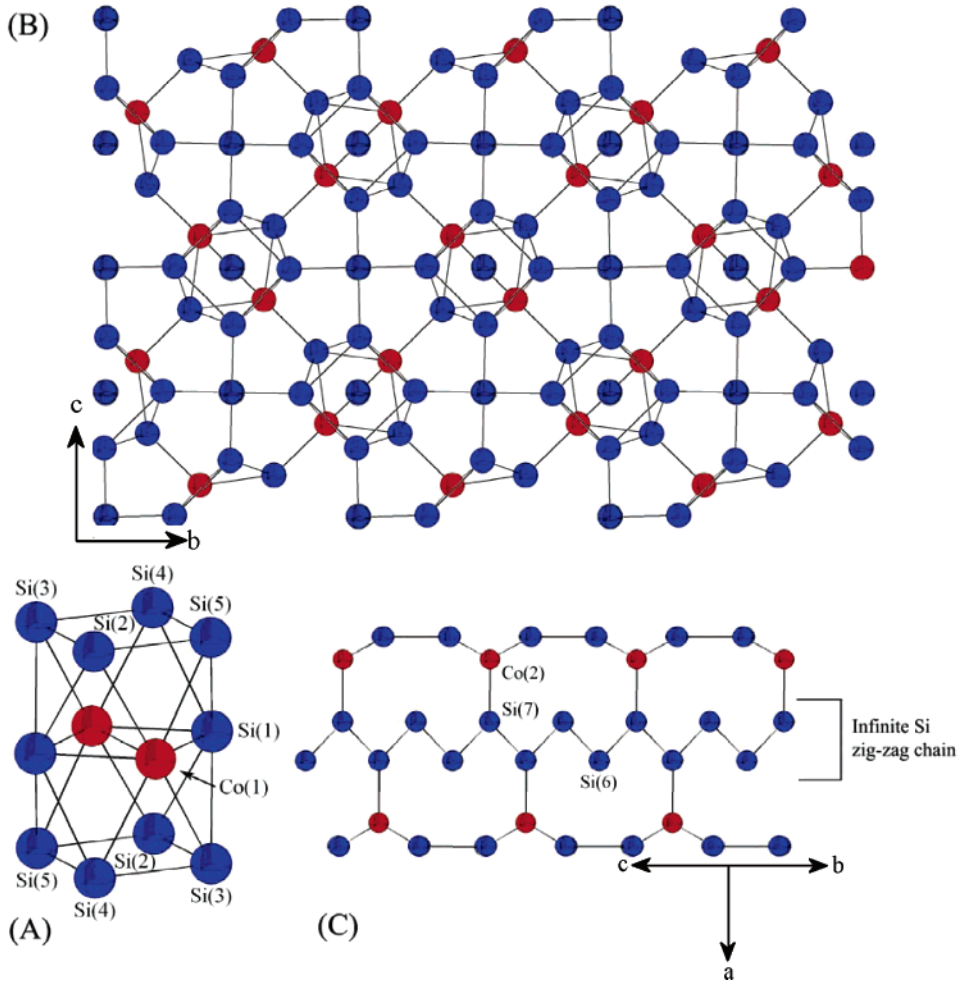

Figure 2. (A) View of a Co_2Si_{10} cage. (B) Structure of $RE_5Co_4Si_{14}$ as viewed down the *a*-axis showing the interconnectivity of the Co_2Si_{10} cages in the *bc*-layer. (C) View of the Si zigzag chains which connect the cages along the *a*-axis; rare earth atoms omitted for clarity.

range from 2.282(3) to 2.292(3) Å for Si(1) to about 2.49 Å for the remaining Si atoms. These cages are connected to one another in the *bc*-plane through two types of bonds to form slabs Figure 2B. One bond is between Co(1) and Si(1) at a distance of 2.269(3) Å and the other is between Co(2) and one of the four crystallographically distinct Si atoms which comprise the top and the bottom of the Co_2Si_{10} cage (Si(2), Si(3), Si(4), and Si(5)) with a distance of approximately 2.3 Å, Figure 2B. The rare earth atoms are omitted from these figures for clarity.

The slabs are interconnected via Co(2) bonding to a Si_4 zigzag chain propagating along the *c*-axis, which then bonds to the slabs below it. Figure 2C is a perspective view along the diagonal bisecting the *b*- and *c*-axes of the zigzag chain which shows that Si(6) forms bonds only to other Si atoms with a distance of 2.419(8) Å for Si(6)−Si(6) and Si(6)−Si(7). Si(7) forms a bond between the chain and the Co(2) atoms with a distance of 2.318(4) Å. These Si−Si distances compare well with other Si-rich compounds such as $SmNiSi_3$ whose Si−Si distances range from 2.344 to 2.409 Å.[13] This bonding results in an alternating stack of slabs and zigzag chains along the *a*-axis, shown in Figure 3. A complete list of bond distances for $Tm_5Co_4Si_{14}$ are given in Table 3. A complete list of the bond distances for $RE_5Co_4Si_{14}$ (RE = Ho, Er, and Yb) can be found in the Supporting Information.

The coordination environments for the three crystallographically distinct Tm atoms can be seen in Figure 4A, B, and C for Tm(1), Tm(2), and Tm(3), respectively. Tm(1) is in an irregular 12-coordinate environment of Si and Co atoms with the following distances: 2 different Tm(1)−Si(1) distances at 2.878(3) Å and 2.895(3) Å, Tm(1)−Si(3) at 3.035 Å, Tm(1)−Si(4) at 3.043(3) Å, Tm(1)−Si(5) at 3.038-(4) Å, and Tm(1)−Co(1) at 3.0348(14) Å. Tm(2) and Tm-(3) are in almost identical coordination environments as Tm(1) is also surrounded by 10 Si and 2 Co atoms.

Chabot and Parthé described the $Lu_5Co_4Si_{14}$ in terms of an intergrowth of 3 slabs including: close-packed Si-centered rare earth prisms, square antiprisms formed by 4 Si atoms and 4 rare earth atoms, and a rare earth centered cuboctahedra of Si and an interstitial Co atom that are interconnected by their corners. Further, they draw relationships between the $Lu_5Co_4Si_{14}$ structure and the $Sc_5Co_4Si_{10}$ and $La_3Co_2Sn_7$ structures.[18]

Thermal Stability and Oxidation Resistance. A remarkable feature of these materials is their apparent extreme inertness to both chemical and thermal attack. Crystals of the title compounds were exposed to concentrated HCl, HNO_3, H_2SO_4, aqua-regia (HCl and HNO_3 in a 3:1 ratio), and 5 M NaOH solution and were found to be completely intact after 2 weeks. The compounds were, however, etched by concentrated HF.

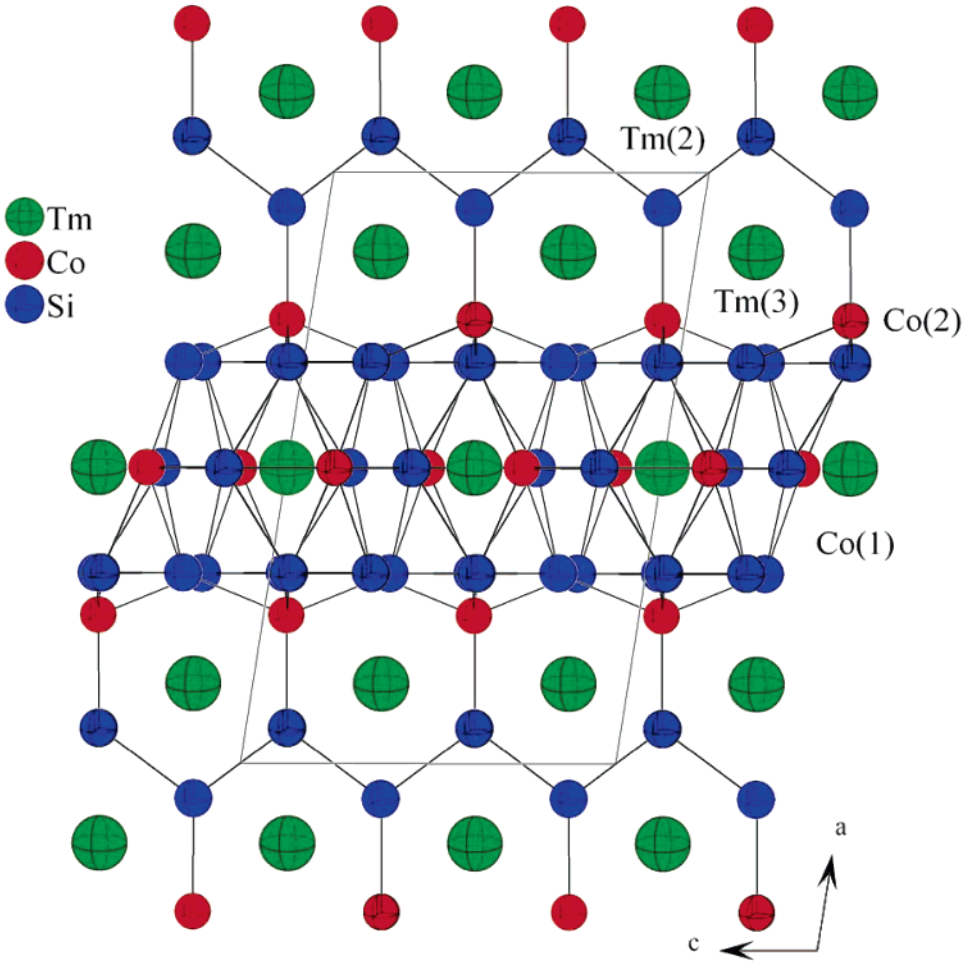

Figure 3. The structure of $RE_5Co_4Si_{14}$ as viewed down the *b*-axis.

Table 3. Bond Lengths [Å] for $Tm_5Co_4Si_{14}$

Tm(1)−Co(1) × 2	3.0347(14)	Co(1)−Co(1)	2.771(2)
Tm(1)−Co(1) × 2	3.0348(14)	Co(1)−Si(1)	2.269(3)
Tm(1)−Co(2) × 2	3.0432(14)	Co(1)−Si(1)	2.283(3)
Tm(1)−Si(1) × 2	2.878(3)	Co(1)−Si(1)	2.292(3)
Tm(1)−Si(1) × 2	2.895(3)	Co(1)−Si(2)	2.493(3)
Tm(1)−Si(2) × 2	3.046(3)	Co(1)−Si(3)	2.484(4)
Tm(1)−Si(3) × 2	3.035(4)	Co(1)−Si(4)	2.491(3)
Tm(1)−Si(4) × 2	3.043(3)	Co(1)−Si(5)	2.485(4)
Tm(1)−Si(5) × 2	3.038(4)	Co(2)−Si(2)	2.301(3)
Tm(2)−Co(2)	3.0681(15)	Co(2)−Si(3)	2.291(4)
Tm(2)−Co(2)	3.0810(16)	Co(2)−Si(4)	2.302(3)
Tm(2)−Si(3)	2.979(3)	Co(2)−Si(5)	2.290(4)
Tm(2)−Si(4)	2.997(3)	Co(2)−Si(7)	2.318(4)
Tm(2)−Si(4)	2.966(3)	Si(1)−Si(2)	2.591(4)
Tm(2)−Si(5)	3.008(3)	Si(1)−Si(3)	2.594(4)
Tm(2)−Si(6)	3.058(3)	Si(1)−Si(4)	2.584(4)
Tm(2)−Si(6)	2.875(3)	Si(1)−Si(5)	2.588(4)
Tm(2)−Si(6)	2.896(3)	Si(2)−Si(3)	2.524(5)
Tm(2)−Si(7)	3.076(3)	Si(2)−Si(5)	2.412(5)
Tm(2)−Si(7)	2.883(3)	Si(3)−Si(4)	2.406(5)
Tm(2)−Si(7)	2.884(3)	Si(4)−Si(5)	2.535(5)
Tm(3)−Co(2)	3.0660(15)	Si(6)−Si(6)	2.419(8)
Tm(3)−Co(2)	3.0816(16)	Si(6)−Si(7)	2.419(7)
Tm(3)−Si(2)	2.957(3)	Si(7)−Si(7)	2.393(8)
Tm(3)−Si(2)	3.008(3)		
Tm(3)−Si(3)	3.019(3)		
Tm(3)−Si(5)	2.970(3)		
Tm(3)−Si(6)	3.070(3)		
Tm(3)−Si(6)	2.867(3)		
Tm(3)−Si(6)	2.904(3)		
Tm(3)−Si(7)	2.890(3)		
Tm(3)−Si(7)	2.892(3)		
Tm(3)−Si(7)	3.052(3)		

In addition $RE_5Co_4Si_{14}$ was found to be quite stable and resistant to thermal oxidation. Differential thermal analysis showed no evidence of a phase change up to 1000 °C. Thermal gravimetric analysis under flowing air was performed on crystals of $Tm_5Co_4Si_{14}$ to determine the extent to which it oxidizes when heated under normal atmospheric conditions. At 1000 °C the material underwent a very small weight gain of 1%, suggesting that the compound does not oxidize appreciably when heated in the atmosphere. The slight weight gain upon heating indicates that whatever oxide is formed during the heating process is not volatile and adheres to the surface of the sample, presumably forming a protective layer.

To more realistically test the resistance to atmospheric corrosion, several crystals of $Tm_5Co_4Si_{14}$ were selected and loaded into open-ended fused silica tubes and annealed in air at 1000 °C for 24 h. Remarkably, this annealing process did not compromise the structural integrity of the compound. Crystal facets were still evident as seen in the SEM micrograph in Figure 5A. It is apparent by visual inspection and elemental analysis that an oxide layer formed on the surface of the crystal as a result of the annealing. Semiquantitative microprobe elemental analysis of the annealed sample reveals elevated levels of Si on the surface as compared to those of the unannealed crystals; also the oxygen Kα line was present in the spectrum, a feature not found in the spectrum of the pristine sample. These findings support the notion of a protective SiO_2 scale forming on the surface of the material, preventing further oxidation below.

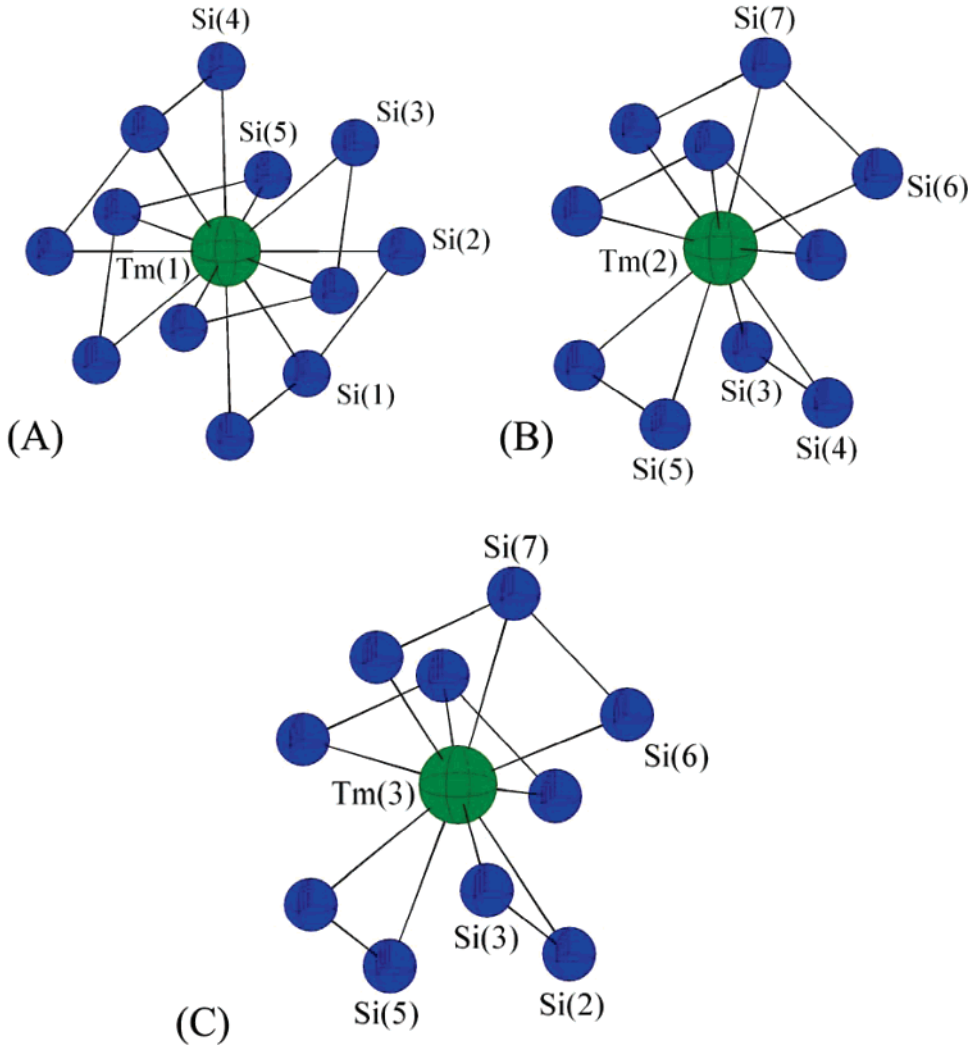

Figure 4. (A) Coordination environment of Tm(1). (B) Coordination environment of Tm(2). (C) Coordination environment of Tm(3).

It is apparent by inspection of Figure 5 that different crystal faces have different scale formations. The single crystal whose faces are numbered in Figure 5A was separated from the annealed cluster, and the faces were indexed by X-ray diffraction. The crystal face labeled 1 was determined to be the (100) face and 2 indexed as the (101) face. The (100) face forms an oxide film that resembles the hooks found in Velcro and showed a larger elevation of Si content as compared to the (101) surface which would suggest that the silicon oxide layer is thicker in the former. The (101) surface showed an increase in the atomic ratios of both Si and Co (15% and 13%, respectively) and has a smoother texture.

The fact that different scales form on different faces upon heating in the presence of oxygen can be understood by considering the species that would likely be present in each of them based on the crystal structure. The (100) faces are likely to have larger amounts of Si present, and thus have a coating that is composed of a thicker SiO_2 layer. Based on the crystal structure, the (101) crystal plane could contain larger amounts of Co and rare earth ions and less Si, and while the protective coating still exists on these faces, it is probably not as thick. These findings suggest differences in the kinetics of oxide formation on the (100) and (101) surfaces likely due to the different chemical species found there. The thinner films found on the (101) surface do not appear to be as bright in the micrographs as they are better conductors.[26]

The protective scale formed on the surfaces of these compounds is a passivating SiO_2 layer, which does not allow transport of oxygen below the surface, thus preventing more extensive corrosion. This suggests that the kinetics of oxide formation in this particular compound are diffusion-controlled, and the rate of oxide layer formation slows as the oxide layer thickens and is effectively halted after a certain critical thickness is obtained.[27]

Reactive metals such as rare earths and some early transition metals have been found to enhance the refractory nature of materials by forming barriers between the SiO_2 layer and the bulk which can both decrease the rate of oxide formation and enhance the adhesion of the oxide layer.[28] This is known as the reactive element effect and implies that more complex ternary or quaternary silicides may be more resistant

(26) The different levels of brightness are from charging effects from the electron beam striking the thicker oxide layer on the (100) face. The (101) face (as well as other crystal faces) having a thinner oxide coating does not charge as much and is therefore not as bright.

(27) Kubaschewski, O.; Hopkins, B. E. *Oxidation of Metals and Alloys I*; Butterworth: London, 1962.

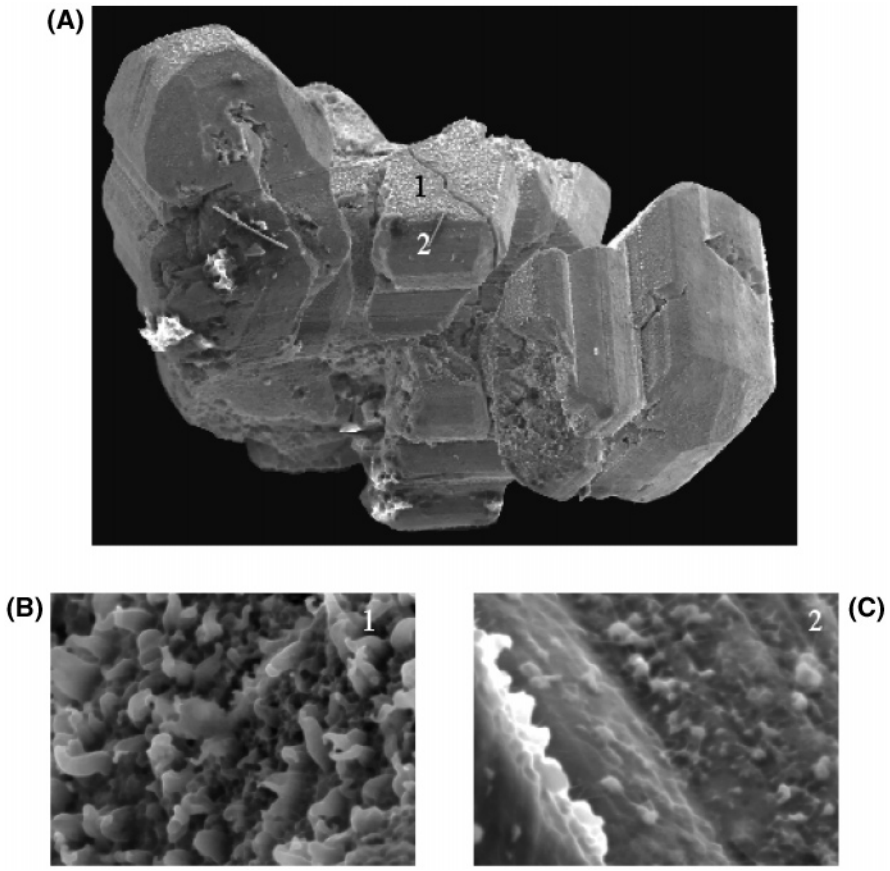

Figure 5. (A) Scanning electron micrograph of $Tm_5Co_4Si_{14}$ after annealing at 1000 °C in an ambient atmosphere for 24 h. (B) Close-up view of crystal face 1. (C) Close-up view of crystal face 2.

than binaries. It is likely the fact that $RE_5Co_4Si_{14}$ is rich in rare earth and transition metal that makes it such a refractory material.

Magnetic Measurements. Magnetic susceptibility and magnetization measurements performed on washed polycrystalline samples of $Ho_5Co_4Si_{14}$, $Er_5Co_4Si_{14}$, $Tm_5Co_4Si_{14}$, and $Yb_5Co_4Si_{14}$ are shown in Figure 6A,B, Figure 6C,D, Figure 7A,B, and Figure 7C,D, respectively. Temperature-dependent magnetic susceptibility of $Ho_5Co_4Si_{14}$ (Figure 6A) obeys the Curie/Weiss law from 300 K to 2 K with a resulting effective magnetic moment of 22.6 μ_B and a Weiss constant (θ) of 5.8 K, indicating weak ferromagnetic interactions.[29] The measured magnetic moment is in reasonably good agreement with that calculated for 5 Ho^{3+} ions, which is 23.7 μ_B. The magnetization data for $Ho_5Co_4Si_{14}$ shows a sharp jump in the magnetization with the application of a small field. Above 500 Oe the moment increases nearly linearly up to 22 kOe, at which point the moment begins to saturate, and slowly increases up to the maximum field of 55 kOe to a value of 21 μ_B. This value is also in good agreement with the expected μ_{sat} value for 5 Ho^{3+} ions, which is 20.5 μ_B.[29] As the field is decreased, there is a small hysteresis in the moment between 20 and 10 kOe. This can be rationalized by imagining the Ho^{3+} moments being aligned by the application of an increasing magnetic field strength; then, as the field is decreased, ferromagnetic interactions keep the moments aligned below the field initially needed to align them, resulting in the hysteresis. As the field is decreased further, below 10 kOe, the ordering is no longer stable, and a more random arrangement of spins is adopted. This model is consistent with the susceptibility data that showed ferromagnetic interactions between the Ho^{3+} ions to be present ($\theta = 5.8$ K), though no ferromagnetic ordering was observed down to 2 K.

The susceptibility data for $Er_5Co_4Si_{14}$ shows a maximum at 4 K, Figure 6C. Above this temperature the data follow the Curie/Weiss law with a resulting effective magnetic moment of 20 μ_B and Weiss constant $\theta = -12$ K, indicating antiferromagnetic interactions consistent with the probable anitferromagnetic ordering at low temperatures. The measured effective magnetic moment for $Er_5Co_4Si_{14}$ (21.4 μ_B) agrees very well with the moment calculated for 5 isolated Er^{3+} ions, which is 21.4 μ_B.[29] The magnetization data for $Er_5Co_4Si_{14}$, Figure 6D, displays a small kink at about 600 Oe followed by a steep increase in the moment with field up to about 15 kOe. Above this field the moments begin to saturate and the field dependence decreases greatly. The moment continues to increase up to 55 kOe, reaching a maximum value of 20 μ_B, which is larger than the calculated μ_{sat} value of 19.0 μ_B. The transition observed in the magnetization data likely corresponds to metamagnetic

(28) (a) Giggen, C. S.; Kear, B. H.; Pettit, F. S.; Tien, J. K. *Metall. Mater. Trans.* **1974**, *5*, 1685. (b) Smialek, J. L. *Metall. Mater. Trans.* **1978**, *9A*, 309. (c) Hindam, H. M.; Smeltzer, W. W. *J. Electrochem. Soc.* **1980**, *127*, 1630.

(29) Kittel, C. *Introduction to Solid State Physics*, 7th ed.; Wiley: New York, 1996; p 425.

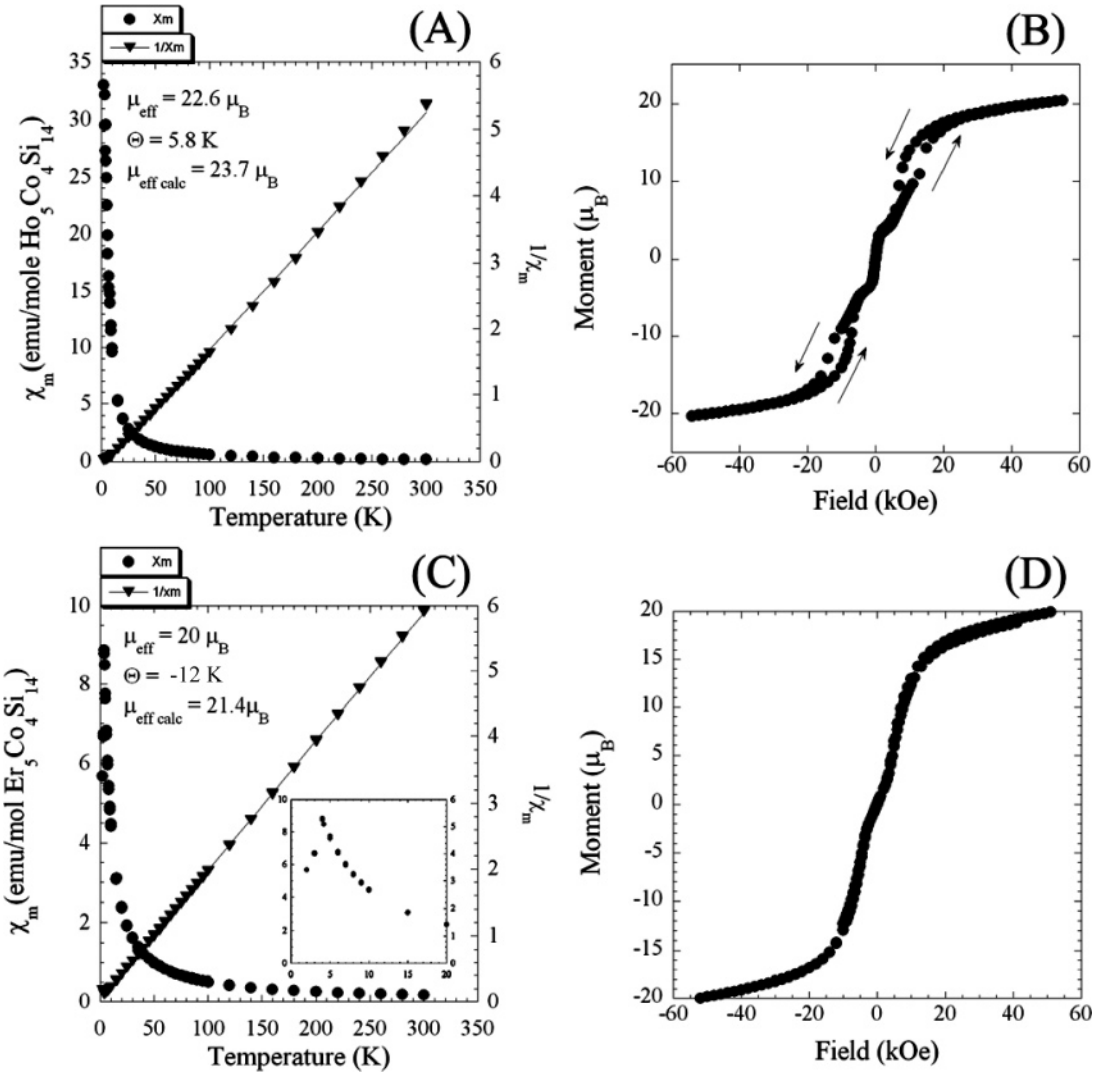

Figure 6. (A) Temperature-dependent magnetic susceptibility of $Ho_5Co_4Si_{14}$. (B) Field-dependent magnetization curve for $Ho_5Co_4Si_{14}$. (C) Temperature-dependent magnetic susceptibility of $Er_5Co_4Si_{14}$. (D) Field-dependent magnetization curve for $Er_5Co_4Si_{14}$.

behavior caused by the applied field, breaking the antiferromagnetic order, thereby causing the moments to align with the field. This results in a ferromagnetic arrangement of the spins, which saturate at high fields. There was no hysteresis found in the magnetization curve.

The susceptibility data for $Tm_5Co_4Si_{14}$ does not show any magnetic ordering and obeys the Curie/Weiss law over a limited temperature range from 2 to 150 K, Figure 7A. The effective magnetic moment obtained from the data in this range was 16.1 μ_B, which compares reasonably well to the calculated moment for 5 Tm^{3+} ions of 17 μ_B.[29] The Weiss constant was very small with a value $\theta = 0.18$ K. The extremely small Weiss constant suggests that there are no significant magnetic interactions between the rare earth ions. Above 150 K the inverse susceptibility negatively diverges, which could be due to crystal field splitting of the $^3H_6$ ground-state multiplet.[30] The magnetization data shows no transitions and no hysteresis. The moment shows strong linear field dependence up to 10 kOe. Above this point the moments begin to saturate with a magnitude of 16 μ_B at 55 kOe. This moment equals the calculated saturation moment for 5 Tm^{3+} ions, indicating that $Tm_5Co_4Si_{14}$ saturates completely.

The susceptibility data for $Yb_5Co_4Si_{14}$, Figure 7C, shows no magnetic ordering down to 2 K. Similar, to the Tm analogue, the data also followed a Curie/Weiss law over a limited temperature range between 50 K and 300 K. These data yield an effective magnetic moment of 10.7 μ_B and a large Weiss constant of $\theta = -41$ K. The effective magnetic moment from the susceptibility measurements agrees well with the value calculated for 5 Yb^{3+} ions, which is 10.2 μ_B. Below 70 K the inverse susceptibility negatively diverges from linearity, and again may be due to crystal field splitting of the $^2F_{7/2}$ multiplet,[30] or as can be the case with Yb a subtle temperature induced valence transition between Yb^{3+} and Yb^{2+} may be occurring. The magnetization was measured only up to 1000 Oe; there was a linear dependence of the moment on field up to 1000 Oe.

Each of the compounds investigated obeyed the Curie or Curie/Weiss law in the major part of the temperature range measured. The observed effective magnetic moments were in good agreement with the moments calculated for isolated 3+ ions of the corresponding rare earth metals. In all cases the Co atoms were diamagnetic, indicative of a filled *d* shell.

(30) Van Vleck, J. H. *The Theory of Electronic and Magnetic Susceptibility*; Oxford University Press: London, 1932.

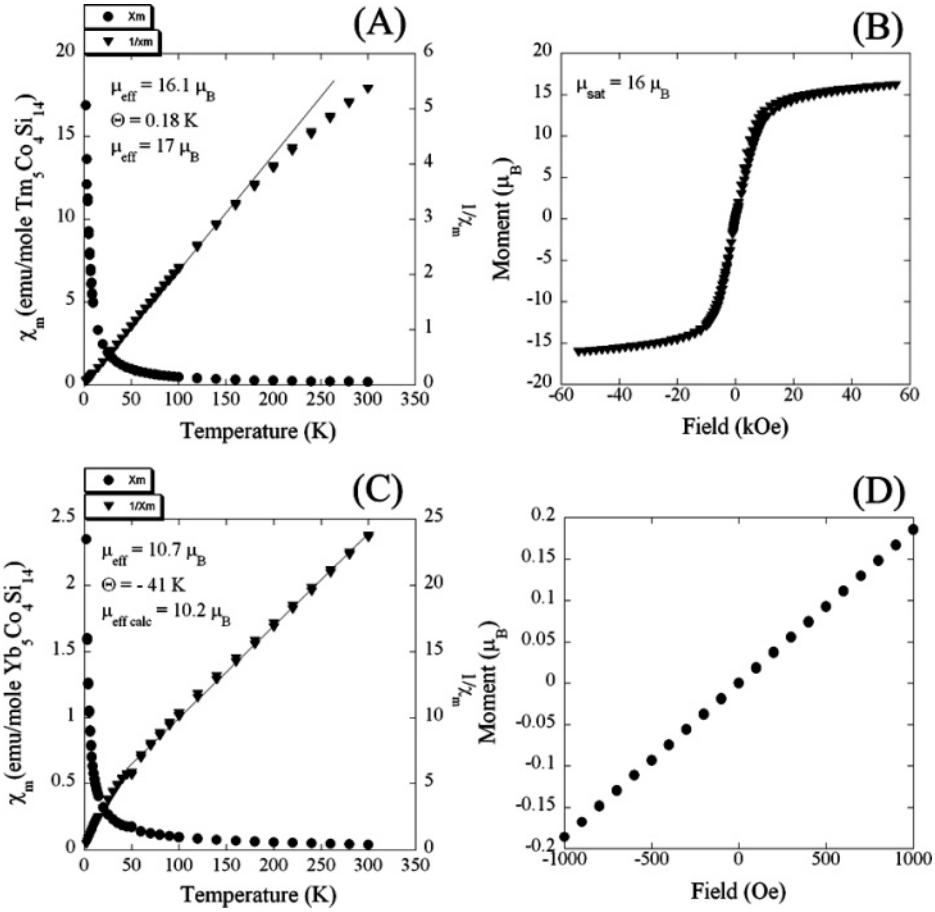

Figure 7. (A) Temperature-dependent magnetic susceptibility of $Tm_5Co_4Si_{14}$. (B) Field-dependent magnetization curve for $Tm_5Co_4Si_{14}$. (C) Temperature-dependent magnetic susceptibility of $Yb_5Co_4Si_{14}$. (D) Field-dependent magnetization curve for $Yb_5Co_4Si_{14}$.

It is common in intermetallic compounds with highly electropositive elements such as rare earth atoms to have late transition metals such as Co and Ni display filled shell diamagnetic behavior.[31]

Concluding Remarks

Liquid Ga has proven to be an excellent non-reactive solvent for synthesizing the ternary silicides $RE_5Co_4Si_{14}$ (RE = Ho, Er, Tm, and Yb) and superior to conventional techniques such as arc melting. The unusual crystal structure of $[Co_4Si_{10}]$ slabs and $^1/_\infty[Si_4]$ zigzag chains arranges the rare earth ions in a diamagnetic matrix where they interact to give rise to a variety of magnetic phenomena. Given the electropositive nature of the RE elements and the results of the magnetic measurements, these compounds can be thought of as polar intermetallics with a charge distribution $(RE^{3+})_5{}^{15+}(Co_4Si_{14})^{15-}$. It is clear from the magnetic measurements that the only paramagnetic contribution to the susceptibility is from the unpaired f electrons of the rare earth ions. The most intriguing property of $RE_5Co_4Si_{14}$ is the remarkable resistance to attack in high-temperature oxidizing environments, as well as harsh chemical conditions such as concentrated acids and bases likely due to the formation of a protective SiO_2 layer. The origin of this behavior can be traced to the details of the monoclinic crystal structure and the Si-rich nature of the crystal framework. The fact that these materials are thermally robust could make possible the growth of thin films via a variety of vapor deposition techniques for surface coatings and related applications. This work suggests that other multinary rare earth transition metal silicides and aluminum silicides may also be particularly refractory.

Acknowledgment. Financial support from the Department of Energy (Grant # DE-FG02-99ER45793 to M.G.K.) is gratefully acknowledged. J.R.G. was a research undergraduate supported by NSF's Summer Research Program in Solid State Chemistry. Part of this work was conducted at the Center for Advanced Microscopy and Center for Sensor Materials at Michigan State University. A generous gift of rare earth elements from Treibacher Industrie AG is gratefully acknowledged.

Supporting Information Available: Crystallographic data (CIF). This material is available free of charge via the Internet at http://pubs.acs.org.

(31) Vajenine, G. V.; Hoffman, R. *J. Am. Chem. Soc.* **1998**, *120*, 4200.

CM047959W